

Scalable Data-Driven Basis Selection for Linear Machine Learning Interatomic Potentials

Tina Torabi^{*§}, Matthias Militzer[†], Michael P. Friedlander[‡], Christoph Ortner[§]

[§] Department of Mathematics, University of British Columbia, Vancouver, V6T1Z2, BC, Canada. *torabit@math.ubc.ca.

[†] The Centre for Metallurgical Process Engineering, University of British Columbia, Vancouver, V6T 1Z4, BC, Canada.

[‡] Department of Computer Science, University of British Columbia, Vancouver, V6T1Z2, BC, Canada.

Abstract—Machine learning interatomic potentials (MLIPs) provide an effective approach for accurately and efficiently modeling atomic interactions, expanding the capabilities of atomistic simulations to complex systems. However, *a priori* feature selection leads to high complexity, which can be detrimental to both computational cost and generalization, resulting in a need for hyperparameter tuning. We demonstrate the benefits of active set algorithms for automated data-driven feature selection. The proposed methods are implemented within the Atomic Cluster Expansion (ACE) framework. Computational tests conducted on a variety of benchmark datasets indicate that sparse ACE models consistently enhance computational efficiency, generalization accuracy and interpretability over dense ACE models. An added benefit of the proposed algorithms is that they produce entire paths of models with varying cost/accuracy ratio.

I. INTRODUCTION

Accurate modeling of interatomic potentials is central to materials simulation. The precision with which interatomic potentials are derived directly impacts the reliability of atomic scale simulations, which are crucial for probing material behavior under diverse conditions [7].

Historically, empirical models such as the embedded-atom method (EAM) [21] and Tersoff potentials [42] have provided computationally efficient means of modeling atomic interactions. However, these models often lack the accuracy and flexibility to describe complex or diverse material and molecular systems. In contrast, first-principles methods like density functional theory (DFT) [10] offer highly accurate representations of atomic interactions but are computationally expensive, restricting their use to relatively small systems or short timescales.

Recent advances in machine learning (ML) have transformed the development of interatomic potentials by combining the accuracy of first-principles methods with the computational efficiency of empirical models. Machine learning interatomic potentials (MLIPs) employ rich descriptors of local atomic environments to construct systematic parameterizations of the potential energy, which is then fitted to match DFT predictions on small snapshots of the system(s) of interest. Early examples include permutation-invariant polynomials [9], neural networks of atom-centered symmetry functions [6], Gaussian approximation potentials [3, 5], the spectral neighbor analysis method (SNAP) [43], moment tensor potentials (MTP) [41], and the atomic cluster expansion (ACE) [25]. Recently, equivariant graph neural network techniques [14, 15, 40, 53] have been gaining increasing traction due to their ability to model vastly more complex systems. However, the focus of the present work will be on linear models; specifically ACE.

For large linear MLIPs models, achieving a balance between model complexity, interpretability, and generalizability remains a challenge [23, 24]. Sparse selection of features can in principle lead to minimal yet informative descriptions. Such models tend to enhance interpretability, scalability, and generalization to unseen configurations. An early example of sparsification in this context appears in the MTP model [41], where a matching pursuit algorithm with crossover and local search was used to minimize an objective with an ℓ_0 regularization term, to train a potential for tungsten. While sparsity was not the primary focus, this work demonstrated that a minimal basis could be identified without sacrificing accuracy. Automatic relevance determination (ARD) [33], an empirical Bayes method that can also be viewed as a sparsification technique, was used in the context of active learning of ACE models [50]. In the present work, we explore the use of two alternative sparse optimization methods, active set basis pursuit (ASP) [27], orthogonal matching pursuit (OMP) [27, 38], and compare them against ARD and various “dense” least squares solvers. The ASP and OMP methods we employ produce entire “paths” of MLIPs models with increasing model complexity. We apply those parameter estimation methods in the linear ACE framework [25].

Our computational tests on three benchmark problems demonstrate several advantages. First, the sparse solvers require minimal user intervention and substantially reduce the need for manual hyperparameter tuning. Secondly, they lead to improved generalization, demonstrated by improved test errors compared to non-sparse solvers. Finally, the selected features do not exhibit a clear or predictable pattern, emphasizing the benefit of data-driven feature selection over heuristic or pre-defined approaches.

II. METHODS

A. Machine Learning Interatomic Potentials (MLIPs)

An atomic configuration is described by a set

$$\mathbf{R} := \{\mathbf{r}_1, \dots, \mathbf{r}_N\} \in \mathbb{R}^{3N},$$

where each \mathbf{r}_j is the position vector of atom j . Defining the displacement between atoms i and j as $\mathbf{r}_{ij} = \mathbf{r}_j - \mathbf{r}_i$, the atomic environment around a reference atom i within a cutoff radius r_c is given by

$$\mathbf{R}_i = \{(\mathbf{r}_{ij}, Z_j) \mid j \neq i, r_{ij} \leq r_{\text{cut}}\},$$

where Z_j is the atomic number of atom j , and $r_{ij} = \|\mathbf{r}_{ij}\|$ is the interatomic distance. An atom is specified by $x_i = (\mathbf{r}_i, Z_i)$ and a bond between atoms i and j is specified by $x_{ij} = (\mathbf{r}_{ij}, Z_i, Z_j)$.

A common approach to constructing interatomic potentials is to decompose the total energy E of the system as a sum of the site energies: $E = \sum_i \epsilon_i$. In linear models, each site energy ϵ_i is expressed as a linear combination of invariant basis functions that encode information about the local environment (e.g., interatomic distances, angles, etc.) within a cutoff radius r_c . The Atomic Cluster Expansion (ACE) framework provides a systematic construction of such models by expanding the site energies in terms of symmetric polynomials, organized by correlation order (or, equivalently, body order) as follows: For a given maximal correlation order $N_{\max} \in \mathbb{N}$, the ACE potential is formulated as

$$\epsilon_i = \sum_{n=0}^{N_{\max}} \sum_{j_1 < j_2 < \dots < j_n} V^{(n)}(x_{ij_1}, x_{ij_2}, \dots, x_{ij_n}),$$

where each many-body interaction $V^{(n)}$ is expanded in a tensor product basis

$$V^{(n)}(x_{ij_1}, \dots, x_{ij_n}) = \sum_{\mathbf{k}} c_{\mathbf{k}}^{(Z_i)} \prod_{s=1}^n \phi_{k_s}(x_{ij_s}), \quad (1)$$

where $\mathbf{k} = (k_1, \dots, k_p)$ and each index k_s corresponds to a tuple $(\mathbf{n}_s, \ell_s, \mathbf{m}_s)$ and the basis functions are defined by

$$\phi_{\mathbf{n}\ell\mathbf{m}}(x_{ij}) = R_{\mathbf{n}\ell}(r_{ij}, Z_i, Z_j) Y_{\ell}^{\mathbf{m}}(\hat{\mathbf{r}}_{ij}).$$

Here, $Y_{\ell}^{\mathbf{m}}$ denote the complex or real spherical harmonics, while $R_{\mathbf{n}\ell}$ are radial basis functions with significant freedom of choice. Detailed implementation aspects, including the choice of the radial basis $R_{\mathbf{n}\ell}$, can be found in [52] and Appendix A.

The invariant basis can then be expressed as:

$$B_{\mathbf{n}\ell q}(\{x_{ij}\}) = \sum_{\mathbf{m}} C_{\mathbf{m}}^{\mathbf{n}\ell q} \prod_s \sum_j \phi_{\mathbf{m}_s \ell_s \mathbf{m}_s}(x_{ij}) \quad (2)$$

where $C_{\mathbf{m}}^{\mathbf{n}\ell q}$ are generalized Clebsch-Gordan coefficients, ensuring $O(3)$ -invariance of $B_{\mathbf{n}\ell q}$. The index $q = 1, \dots, n_{\mathbf{n}\ell}$ enumerates all invariant couplings; see [1] for more details.

This leads to the final linear parameterization of the ACE potential

$$\epsilon_i = \sum_{B \in \mathbf{B}} c_B B(\{x_{ij}\}),$$

where c_B are the model parameters and \mathbf{B} is a finite set of basis functions

$$\begin{aligned} \mathbf{B} := \left\{ B_{\mathbf{n}\ell q} \mid (\mathbf{n}, \ell) \in \mathbb{N}^{2N} \text{ (ordered)}, \sum_{\alpha} \ell_{\alpha} \text{ even}, \right. \\ \left. \sum_{\alpha} m_{\alpha} = 0, q = 1, \dots, n_{\mathbf{n}\ell}, \right. \\ \left. \sum_{\alpha} (\ell_{\alpha} + \mathbf{n}_{\alpha}) \leq D_{\text{tot}}, N \leq N_{\max} \right\}. \end{aligned}$$

The completeness of this representation implies that, as the approximation parameters N_{\max} (correlation order), r_{cut} (cutoff radius), and D_{tot} (expansion precision) tend to infinity, the model is capable of representing any arbitrary potential [1]. Although these parameters provide a systematic way to refine the approximation, manually selecting them through heuristics or grid searches introduces a major bottleneck in model development. Even if optimal parameters can be selected, this does not result in an optimal or even near-optimal choice of basis,

which would require selection of individual basis functions. Rather than fine-tuning hyperparameters manually, the goal of our framework is to eliminate the need for exhaustive hyperparameter tuning by performing automatic feature selection, ensuring that only the most informative basis functions are directly selected during parameter estimation. We will demonstrate in several examples that this data-driven approach increases automation, reduces computational overhead and enhances generalization, stability, and interpretability of the resulting interatomic potential.

Parameter Estimation and Regularization: To estimate the coefficients \mathbf{c} , a training dataset of atomic configurations $\mathfrak{R} = \{\mathbf{R}\}$ is required. For each configuration \mathbf{R} , target potential energy $\mathcal{E}_{\mathbf{R}}$, forces $\mathcal{F}_{\mathbf{R}}$ and virials $\mathcal{V}_{\mathbf{R}}$ are provided, usually from DFT calculations. The model parameters are then obtained by minimizing a least-squares loss function:

$$\begin{aligned} L(\mathbf{c}) = \sum_{\mathbf{R} \in \mathfrak{R}} \left(w_{E,\mathbf{R}}^2 |E(\mathbf{c}; \mathbf{R}) - \mathcal{E}_{\mathbf{R}}|^2 \right. \\ \left. + w_{F,\mathbf{R}}^2 |F(\mathbf{c}; \mathbf{R}) - \mathcal{F}_{\mathbf{R}}|^2 \right. \\ \left. + w_{V,\mathbf{R}}^2 |V(\mathbf{c}; \mathbf{R}) - \mathcal{V}_{\mathbf{R}}|^2 \right). \end{aligned}$$

Here, the weights $w_{E,\mathbf{R}}$, $w_{F,\mathbf{R}}$, and $w_{V,\mathbf{R}}$ assign varying levels of importance to different observations and structures. In all our tests we use the defaults published in [52]. The coefficients \mathbf{c} are obtained by solving the minimization problem:

$$\mathbf{c} = \arg \min_{\mathbf{c}} \|\mathbf{W}(\mathbf{y} - \mathbf{A}\mathbf{c})\|_2^2,$$

where \mathbf{y} collects the observed data (energies, forces, stresses), \mathbf{A} is the design matrix composed of basis function values, and \mathbf{W} is a diagonal matrix that can be used to specify chosen weights.

To avoid overfitting, one typically employs regularized modifications such as ridge or Bayesian regression. In the context of ACE MLIPs, a natural approach to regularize is to encourage “smoothness” of the fitted potential, or equivalently, avoid oscillatory behavior that are common when overfitting polynomials. Concretely, we employ an *algebraic smoothness prior* introduced in [2, 52]. Each basis function, indexed by $\{n_t, \ell_t\}$, is assigned a smoothness cost:

$$\gamma_{\mathbf{n}\ell\mathbf{m}}(p) = \sum_t (n_t^p + w_L \ell_t^p),$$

where w_L balances the contributions of the radial and angular components; we again use defaults from [52]. These costs are assembled into a diagonal matrix Γ (with $\Gamma_{kk} = \gamma_k$) and incorporated into the regularized minimization:

$$\arg \min_{\mathbf{c}} \|\mathbf{W}(\mathbf{y} - \mathbf{A}\mathbf{c})\|^2 + \lambda \|\Gamma \mathbf{c}\|^2.$$

Higher values of λ or γ_k favor smoother, less oscillatory potentials. The `ACEpotentials.jl` package [52] provides additional smoothness priors—such as the exponential and Gaussian priors—that offer varying degrees of penalization on oscillatory terms.

The `ACEpotentials.jl` package [52] also offers a range of solvers tailored for different dataset sizes and computational requirements. Once the model parameters are determined, the next step is to validate the potential on a test dataset. Common metrics for evaluating accuracy include the root mean square

error (RMSE) and mean absolute error (MAE) for energies, forces, and stresses. Following successful validation, the model can be exported in various formats for subsequent use in molecular dynamics simulations.

B. Sparse recovery methods

Least-squares (LS) problems, such as (3), arise in numerous applications across signal processing, data science, and machine learning [26, 32]. In a standard LS problem, the objective is to solve for a vector $x \in \mathbb{R}^n$ that minimizes the residual $\|Ax - b\|_2^2$, where $A \in \mathbb{R}^{m \times n}$ is a known matrix, often termed a dictionary, and $b \in \mathbb{R}^m$ is the target vector. Sparse solutions, where most entries in x are zero or near-zero, are particularly desirable in scenarios where only a small subset of predictors or signal components is relevant. Sparse solutions have important implications in model selection as they enable the identification of minimal predictor subsets that improve both interpretability and model generalization [44]. In signal processing, they facilitate signal reconstruction from limited measurements by assuming the signal is representable in a sparse basis [35]. Compressed sensing leverages sparsity to efficiently acquire and reconstruct signals from a reduced set of samples, thereby reducing data acquisition costs [11].

In optimization terms, the goal is to identify the smallest possible subset of *features* from the set represented by the columns of the matrix A . A sparse solution x thus corresponds to selecting the minimal set of features that best approximates the target vector b . Formally, this sparse approximation problem, referred to as the Sparse Approximate Solution (SAS) problem, can be stated as follows: Given a matrix $A \in \mathbb{R}^{m \times n}$, where A has m rows and n columns, a target vector $b \in \mathbb{R}^m$, and a tolerance $\epsilon > 0$, find a vector x that satisfies

$$\|Ax - b\|_2 \leq \epsilon$$

and has the fewest possible nonzero entries among all vectors satisfying this condition. The sparse approximation selection (SAS) problem is known to be NP-hard [36]. However, practical alternatives exist, often classified into three main categories: convex relaxations, non-convex optimization techniques, and greedy algorithms. In what follows we will briefly review a few of these alternatives.

1) *Convex relaxations*: Convex relaxations techniques provide practical alternatives for solving SAS and under specific conditions, can effectively approximate or even recover the exact sparsest solution [12]. A common approach is to formulate the problem using the ℓ_1 -norm objective and linear constraints (Basis Pursuit, BP [16]) or as a regularized least-squares problem (Basis Pursuit Denoising, BPDN [17]), or as the Least Absolute Shrinkage and Selection Operator (LASSO) [45]. The duals of these problems can be formulated as conventional linear and quadratic programs [49]. Consider the following primal and dual optimization problems:

$$\begin{aligned} \textbf{Primal:} \quad & \underset{x,y}{\text{minimize}} \quad \|x\|_1 + \frac{1}{2}\lambda\|y\|_2^2 \\ & \text{subject to} \quad Ax + \lambda y = b, \\ \\ \textbf{Dual:} \quad & \underset{y}{\text{maximize}} \quad b^T y - \frac{1}{2}\lambda\|y\|_2^2 \\ & \text{subject to} \quad -\mathbf{1} \leq A^T y \leq \mathbf{1}, \end{aligned} \tag{3}$$

where $\lambda \geq 0$ is a scalar parameter and $\mathbf{1}$ is a vector of ones. When $\lambda = 0$, this formulation is equivalent to the BP problem. For $\lambda > 0$, the problem represents the BPDN problem. The primal and dual problems are duals of each other in the sense that there exists an optimal pair (x, y) that simultaneously satisfy the Karush-Kuhn-Tucker (KKT) [30, 31] conditions for both problems. Various algorithms have been proposed for solving BP and BPDN. The BP-simplex algorithm [17], inspired by the simplex method in linear programming [51], begins by selecting an initial basis $A^{(0)}$ consisting of m linearly independent columns of A . At each iteration, a swap is made to optimize the objective function by exchanging one term in the basis with one term outside the basis.

Friedlander and Saunders [27] introduced the parameterization (3) of the BPDN problem, based on a dual active-set approach suitable for large-scale problems, as it requires only matrix-vector products. Their algorithm iteratively identifies the active set of constraints, solves a least-squares subproblem on those constraints, and updates the solution estimate by moving along a descent direction. The algorithm continues until it reaches a stationary point where the objective gradient is a linear combination of the gradients of the active constraints, indicating optimality. We describe this algorithm in more detail in Appendix B.

The orthogonal matching pursuit (OMP) [38] algorithm is a greedy algorithm that iteratively builds a solution to the problem

$$\underset{x}{\text{minimize}} \quad \|Ax - b\|_2^2 \quad \text{subject to} \quad \|x\|_0 \leq k$$

by selecting the column of A most correlated with the current residual. After selecting a column, OMP updates the solution by solving a least-squares problem using the selected columns and computes a new residual orthogonal to the selected columns. OMP continues this process, adding one column at a time, until a stopping criterion is met, such as achieving a desired residual norm or reaching a predetermined number of iterations. The details of OMP will be discussed in Appendix D.

The Homotopy method [37] is a technique for solving sparse least-squares problems by solving a sequence of LASSO problems with increasing regularization parameters τ_k :

$$\underset{x}{\text{minimize}} \quad \|Ax - b\|_2^2 \quad \text{subject to} \quad \|x\|_1 \leq \tau_k.$$

Homotopy balance the ℓ_1 norm of the solution against the least-squares fit. As the regularization parameter decreases, the solution becomes sparser. This algorithm proceeds by identifying breakpoints, which are specific values of τ_k where the set of non-zero variables changes. The solution is updated systematically as τ_k passes through each breakpoint. We describe the Homotopy algorithm in more detail in Appendix C.

2) *Empirical Bayes methods*: Bayesian ridge regression (BRR) [22, 34] is a probabilistic approach to linear regression that uses a Bayesian framework to estimate the posterior distribution of the regression coefficients. By modeling the noise and prior distributions as Gaussians, BRR obtains a closed-form solution for the posterior. Automatic relevance determination (ARD) [33] extends this framework by assigning individual precision hyperparameters to each coefficient, thereby facilitating automatic feature selection.

Given the linear model

$$b = Ax + \epsilon,$$

where the error $\epsilon \sim \mathcal{N}(\mathbf{0}, \lambda^{-1}\mathbf{I})$, the likelihood function is

$$p(b | A, x, \lambda) = \left(\frac{\lambda}{2\pi}\right)^{m/2} \exp\left(-\frac{\lambda}{2}\|b - Ax\|^2\right).$$

A Gaussian prior is placed on the regression coefficients:

$$p(x | \alpha) = \mathcal{N}(x | \mathbf{0}, \alpha^{-1}\mathbf{I}), \quad (4)$$

resulting in a Gaussian posterior

$$p(x | b, A, \alpha, \lambda) = \mathcal{N}(x | \hat{x}, \Sigma),$$

with:

$$\begin{aligned} \Sigma &= (\alpha\mathbf{I} + \lambda A^\top A)^{-1}, \\ \hat{x} &= \lambda \Sigma A^\top b. \end{aligned}$$

Hyperparameters α and λ are typically optimized via evidence maximization.

Automatic relevance determination (ARD) generalizes (4) by assigning an independent precision α_i to each coefficient:

$$p(x | \alpha) = \mathcal{N}(x | \mathbf{0}, \Gamma^{-1}),$$

where the covariance matrix is

$$\Gamma = \text{diag}(\alpha_1, \alpha_2, \dots, \alpha_{N_{\text{basis}}}).$$

This selective regularization facilitates feature selection by effectively shrinking irrelevant coefficients toward zero.

In the context of ACE MLIPs, ARD has been used within the Hyperactive Learning (HAL) framework [50]. After fitting the model, posterior samples of the model parameters are drawn, and a committee of ACE models is formed to efficiently approximate the uncertainty in energy and force predictions. This uncertainty is then used in the HAL loop to identify configurations where the model is least certain. For further details on the derivations and optimization, refer to Appendix E.

III. RESULTS

We present a number of benchmark results to test the proposed parameter estimation methods. In all benchmarks, a dataset was divided into training, validation, and test sets. The best checkpoint model was identified as the one achieving the lowest error on the validation set. For models of size t , the best checkpoint corresponds to the model with the best validation performance while having at most t basis functions in the active set. These checkpoint models were then used to evaluate performance on the test set. In this section, we refer to the homotopy LASSO solver and the Orthogonal Matching Pursuit solver, introduced in Section II-B1, respectively, as ASP and OMP. We employ a Julia implementation `ActiveSetPursuit.jl` [47] of the BPdual, Homotopy, and OMP algorithms, based on [29].

An artifact of the BPDN model is its tendency to shrink coefficients toward zero as a result of the ℓ_1 -regularization. To de-bias [48, 54] the model, we applied a post-processing step using truncated singular value decomposition (TSVD) to refine the final coefficients. TSVD mitigates this issue by projecting the solution onto a lower-dimensional subspace, filtering out

small singular values that contribute to numerical instability while preserving the dominant structures in the solution. This post-processing step thus improves both the accuracy and robustness of the final coefficient estimates. Further details on the TSVD procedure and its effects on the results can be found in Appendix F.

Apart from test errors, a key indicator of a machine-learned interatomic potential's quality is its stability—the ability to sustain long molecular dynamics (MD) simulations while ensuring the system remains in physically meaningful states without divergence or instability. To assess the stability of the ACE potentials, we conducted NVT MD simulations on test set configurations at 300K and 500K, using a 5-femtosecond timestep over a 1-nanosecond trajectory for metals and semi-metals, and a 1-femtosecond timestep over a 1-nanosecond trajectory for water. Our results confirmed the stability of *all* fitted ACE potentials under these conditions. For more details please refer to *Supplementary Information*.

A summary of all the solvers used within this section and their most appropriate use cases is shown in Table I. This table provides a concise overview of each solver's methodology, along with guidance on when it is most applicable for different problem settings. For each set of results we compare sparse solvers to a reference dense solver employed in previous tests in [52].

A. Limited diversity metal datasets

We evaluate the performance of the ASP and OMP solvers with default parameters on several low-diversity datasets, which arise for example in automated workflows that require special purpose potentials for a limited range of tasks, in particular (hyper-)active learning. We employ the single-element benchmarks [55] including six datasets for, respectively, Li, Mo, Ni, Cu, Si, and Ge. These elements cover a range of chemical properties (main group metals, transition metals, and semiconductors), crystal structures (bcc, fcc, and diamond), and bonding types (metallic and covalent). Each dataset comprises the element's ground-state crystal structure, strained configurations with strains ranging from -10% to 10% , slab structures with Miller indices up to three, and NVT *ab initio* molecular dynamics simulations of bulk supercells, both with and without a single vacancy. We refer to [55] for further details. While the datasets provide a large number of training structures, they exhibit limited diversity compared to more recent MLIPs training sets.

Our starting basis size was approximately 5000 (corresponding to a D_{tot} of 25 and N_{max} of 3). We then allowed OMP, ASP, and the ARD solver from scikit-learn [39] to select the most relevant basis functions. We terminated ASP and OMP when the number of active elements hit 300 for the small model and 1000 for the large model. We also obtained the ARD solutions with desired sparsity by modifying α . The resulting MAE errors of the potentials trained are compared to the previous results reported in [52]. As can be seen from the Tables IIa, IIb, apart from Li where the RRQR solver outperforms OMP and ASP, which suggests that fine-tuning of the model parameters could be beneficial, the OMP and ASP solvers outperform all other elements' best checkpoint reported in [52].

TABLE I: Summary of solvers used for ACE model construction.

| Solver | Description |
|--------|--|
| RRQR | Rank-revealing QR decomposition with random matrix sketching; removes sensitive subspaces based on $rtol$, which is related to λ (Eq. 3) [13]. More performant than standard QR for large datasets. |
| BLR | Bayesian linear regression; selects λ (Eq. 3) via Bayesian evidence maximization [22, 34]. More robust than RRQR but more computationally intensive. Best for small datasets and uncertainty quantification. |
| ARD | Empirical Bayes method with hierarchical sparsity constraints to prune basis functions [33]. |
| ASP | Homotopy solver for LASSO; refines active basis set along a continuous path [27]. Scalable and well-suited for large datasets requiring structured sparsity selection. |
| OMP | Greedy sparse regression method, selecting the most relevant basis functions iteratively [27]. More computationally efficient than ASP. |

TABLE II: Mean absolute test errors in predicted energies (meV) and forces (eV/Å) for small ACE models (≈ 300 basis functions) and large ACE models (≈ 1000 basis functions) using different solvers, compared to the two best-performing MLIPs reported in [55].

(a) Mean absolute test errors in predicted energies (meV).

| Element | Small model [meV] | | | | Large model [meV] | | | | MTP | GAP |
|---------|-------------------|-------|-------|-------|-------------------|-------|-------|-------|------|------|
| | RRQR | ASP | OMP | ARD | RRQR | ASP | OMP | ARD | | |
| Ni | 0.416 | 0.220 | 0.232 | 0.561 | 0.34 | 0.253 | 0.241 | 0.321 | 0.42 | 0.48 |
| Cu | 0.292 | 0.232 | 0.269 | 0.826 | 0.228 | 0.217 | 0.194 | 0.315 | 0.46 | 0.41 |
| Li | 0.231 | 0.373 | 0.345 | 0.438 | 0.165 | 0.355 | 0.354 | 0.319 | 0.49 | 0.49 |
| Mo | 2.597 | 2.261 | 2.123 | 3.945 | 2.911 | 2.138 | 1.933 | 2.381 | 2.24 | 2.83 |
| Si | 3.501 | 2.444 | 2.296 | 3.891 | 2.388 | 1.981 | 1.859 | 2.344 | 2.91 | 2.21 |
| Ge | 2.594 | 2.212 | 1.849 | 2.630 | 2.162 | 2.018 | 1.936 | 2.093 | 2.06 | 1.79 |

(b) Mean absolute test errors in predicted forces (eV/Å).

| Element | Small model [eV/Å] | | | | Large model [eV/Å] | | | | MTP | GAP |
|---------|--------------------|-------|-------|-------|--------------------|-------|-------|-------|------|------|
| | RRQR | ASP | OMP | ARD | RRQR | ASP | OMP | ARD | | |
| Ni | 0.018 | 0.014 | 0.014 | 0.026 | 0.015 | 0.014 | 0.013 | 0.019 | 0.02 | 0.01 |
| Cu | 0.007 | 0.006 | 0.005 | 0.019 | 0.005 | 0.005 | 0.005 | 0.014 | 0.01 | 0.01 |
| Li | 0.006 | 0.008 | 0.008 | 0.056 | 0.005 | 0.007 | 0.007 | 0.008 | 0.01 | 0.01 |
| Mo | 0.123 | 0.104 | 0.098 | 0.138 | 0.097 | 0.087 | 0.086 | 0.092 | 0.09 | 0.09 |
| Si | 0.086 | 0.074 | 0.072 | 0.086 | 0.066 | 0.061 | 0.059 | 0.060 | 0.07 | 0.06 |
| Ge | 0.064 | 0.059 | 0.056 | 0.072 | 0.051 | 0.049 | 0.047 | 0.049 | 0.05 | 0.05 |

Figure 1 shows a comparison of the MAE for energy predictions between OMP, ASP, RRQR, and ARD for the Mo, Ni, and Si datasets as the number of active basis functions increases. OMP and ASP solvers consistently achieve lower MAE than RRQR and ARD as the basis size increases, outperforming them for the majority of the range. Among the solvers in ActiveSetPursuit, while OMP achieves lower errors, ASP appears to be more stable, with OMP exhibiting some fluctuations. Since OMP and ASP significantly outperform ARD, we will present results only for OMP and ASP in subsequent sections.

Figures 2 and 3 visualize the basis functions selected by the ASP solver for, respectively, the two-body and three-body interactions. The patterns of selected basis functions are non-intuitive and deviate significantly from any common *a priori* basis selection mechanism such as total degree or hyperbolic cross selections. This highlights the significant potential benefits of applying data-driven basis selection methods.

B. Silicon (PRX, 2018)

We employed the ASP and OMP solvers to fit a linear ACE potential to the silicon dataset presented in [4], originally developed for training a Gaussian approximation potential (GAP). This dataset is comprehensive, encompassing a diverse range of configurations, including various bulk crystal structures (e.g., diamond, hcp, and fcc), amorphous phases, and liquid molecular dynamics (MD) snapshots. Its goal is to capture a wide range of the elemental silicon energy landscape. Accurate fits to this dataset provide (near-)general-purpose potentials for elemental silicon.

Four models were evaluated: the GAP model and three ACE models trained with default parameters. The ACE model trained using BLR employed basis functions with a maximum correlation order of $N_{\max} = 3$, a total polynomial degree of $D_{\text{tot}} = 20$, and a cutoff radius of $r_c = 6$ Å, resulting in a basis size of 5,434.

Additionally, two more ACE models were trained using ASP and OMP, both with the same maximum correlation order of 3 but a higher total degree of $D_{\text{tot}} = 23$, yielding a larger initial

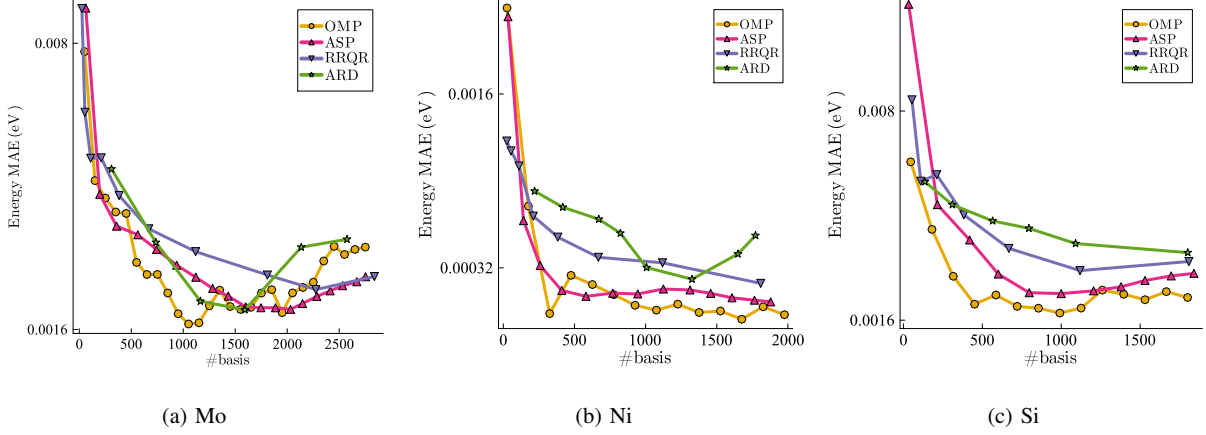


Fig. 1: Energy MAE vs basis size for selected limited diversity datasets (cf. III-A), comparing three sparse least squares solvers (ARD, ASP, OMP) with a direct regularized least squares approach (RRQR).

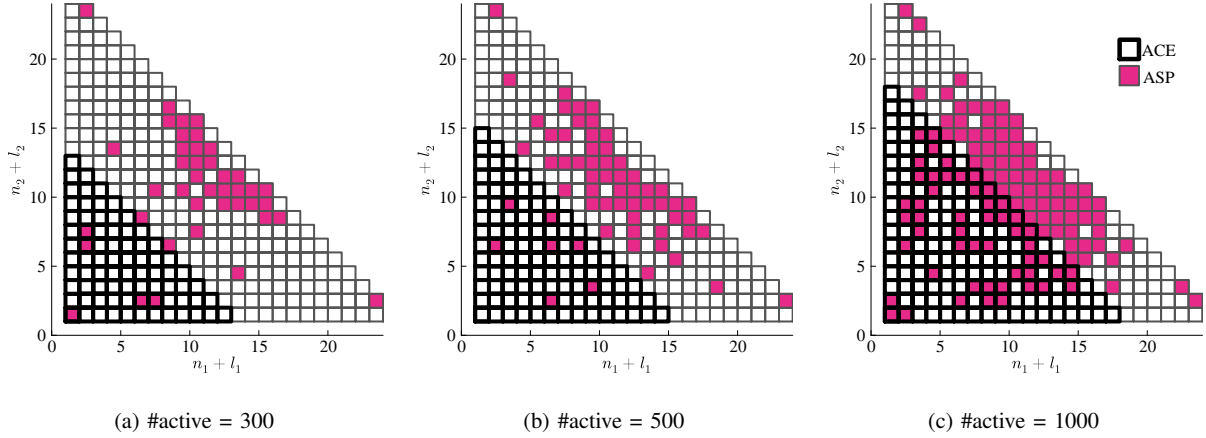


Fig. 2: Visualization of the basis functions selected for two-body interactions in the Mo dataset (cf. III-A). The figure illustrates the gradual selection process of ASP and non-sparse ACE solvers as the number of active basis functions increases. The ASP-selected basis functions (pink) show a distinct, data-driven selection pattern compared to the full ACE basis (black), demonstrating the benefits of data-driven basis selection.

basis size of 13,695. In both cases, training was stopped once 5,000 active basis functions had been selected.

An algebraic smoothness prior Γ with $p = 5$ was employed in all ACE models. Figure 4 illustrates the comparison of energy Mean Absolute Error (MAE) between the ASP, OMP, and BLR solver, across varying basis sizes. In the small basis regime, the BLR, OMP, and ASP solvers exhibit comparable performance in terms of test error. As the basis size increases, the ASP and OMP solver consistently achieve moderately lower test errors compared to BLR, which indicates that selecting an effective subset of basis functions leads to better generalization and less risk of overfitting, even in the current setting with a highly diverse dataset.

A key property of a robust interatomic potential is its out-of-distribution generalization performance. To evaluate this, the benchmark suite of property predictions from [4] was

performed. It includes bulk diamond elastic constants, vacancy formation energies, surface formation energies for the (100), (110), and (111) surfaces, as well as formation energies for hexagonal, dumbbell, and tetragonal point defects in bulk diamond. The reference values for these properties were obtained via CASTEP [20] density functional theory (DFT) calculations.

For comparison, we included results from the GAP potential trained in [4] and the ACE BLR potential trained in [52]. The computed values of these properties are summarized in Table III. These results demonstrate that the ASP and OMP solvers achieve accuracy comparable to the GAP potential and the ACE model trained using BLR, even when training is stopped at 2,500 basis functions—less than 50% of the 5,434 basis functions used by the BLR-trained model.

The corresponding percentage errors of point defect energies relative to the DFT reference values are presented in Figure 5.

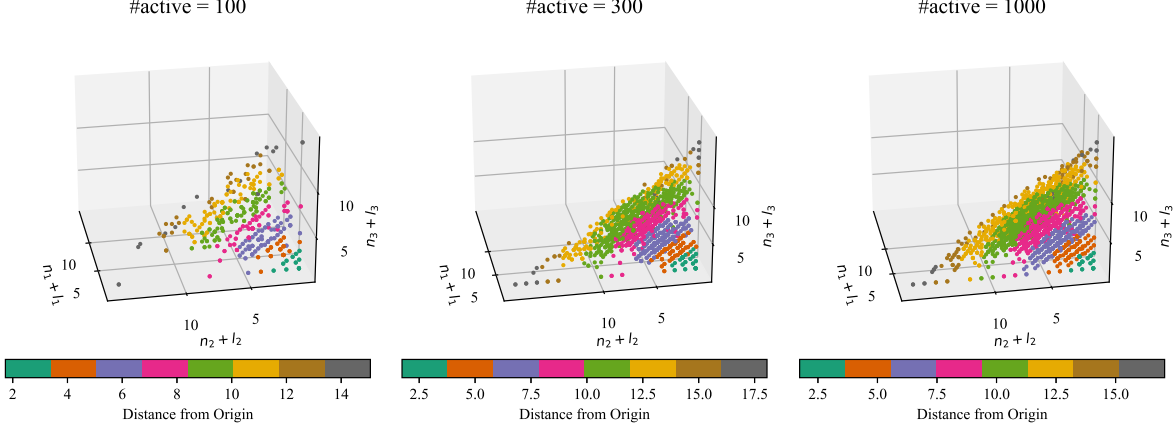


Fig. 3: Visualization of the basis functions selected for three-body interactions in the Mo dataset (cf. III-A). The figure illustrates the gradual selection process of ASP and non-sparse ACE solvers as the number of active basis functions increases. The selection is visualized in 3D, with colors indicating the distance from the origin. Similarly as with 2-correlation, ASP selects features without any a priori predictable pattern.

TABLE III: Comparison of point defects, elastic properties, and surface energies for silicon using DFT, GAP, BLR, ASP, and OMP models (cf. III-B). Models were fitted to the dataset in [4], with reference values obtained from CASTEP [20] density functional theory (DFT) calculations.

| Method | Point Defects [eV] | | | | Elastic Properties [GPa] | | | | Surface Energy [J/m ²] | | |
|------------|--------------------|-----------|------------|------|--------------------------|----------|----------|----------|------------------------------------|-------|-------|
| | Tet. Int. | Hex. Int. | Dumb. Int. | Vac. | B | c_{11} | c_{12} | c_{44} | (111) | (110) | (100) |
| DFT | 3.91 | 3.72 | 3.66 | 3.67 | 88.6 | 153.3 | 56.3 | 72.2 | 1.57 | 1.52 | 2.17 |
| GAP | 3.71 | 3.63 | 3.68 | 3.53 | 88.5 | 151.9 | 63.1 | 99.1 | 1.54 | 1.55 | 2.13 |
| BLR | 3.74 | 3.61 | 3.72 | 3.52 | 88.1 | 156.4 | 60.9 | 102.1 | 1.52 | 1.88 | 2.13 |
| ASP (2500) | 3.70 | 3.66 | 3.73 | 3.51 | 88.3 | 157.7 | 59.9 | 101.3 | 1.52 | 1.87 | 2.13 |
| OMP (5000) | 3.72 | 3.63 | 3.62 | 3.51 | 88.2 | 155.9 | 60.2 | 102.1 | 1.52 | 1.88 | 2.13 |
| ASP (5000) | 3.72 | 3.67 | 3.78 | 3.53 | 88.3 | 156.6 | 60.2 | 102.0 | 1.52 | 1.87 | 2.13 |

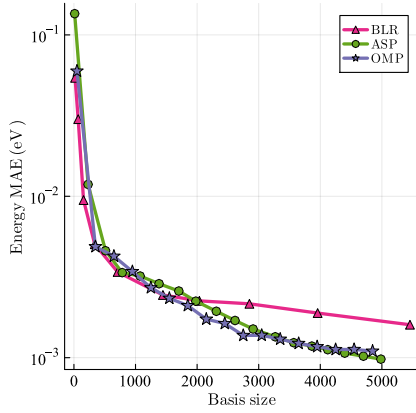


Fig. 4: Energy MAE vs. basis size for the Silicon dataset [4], comparing OMP, BLR, and ASP (cf. III-B). In the mid-to-high basis size regime, ASP and OMP achieve similar or better accuracy than BLR while using significantly fewer basis functions.

The test illustrates how the accuracy of the model improves as the number of basis functions increases. This monotonicity of the error highlights the robustness of ASP for basis selection. Again we observe comparable or better accuracy than BLR while using significantly fewer basis functions. The result further underscores the advantage of sparsity-promoting solvers in balancing computational cost and predictive accuracy, demonstrating that a well-chosen subset of basis functions is sufficient for reliable property predictions.

The basis selection patterns produced by the BLR and ASP solvers for the silicon dataset are similar to those observed in the previous section. Detailed visualizations can be found in the *Supplementary Information*.

C. Water

We utilize OMP and ASP to fit an interatomic potential to a dataset containing 1593 liquid water configurations [18]. In this case, we can test the selection of how basis functions acting between different elements are selected. The model employed default parameters, including basis functions up to a correlation order of $N_{\max} = 3$, a maximum polynomial degree of $D_{\text{tot}} = 15$, and a cutoff radius of $r_c = 5.5 \text{ \AA}$. An algebraic smoothness prior Γ with $p = 4$ was employed in all ACE models.

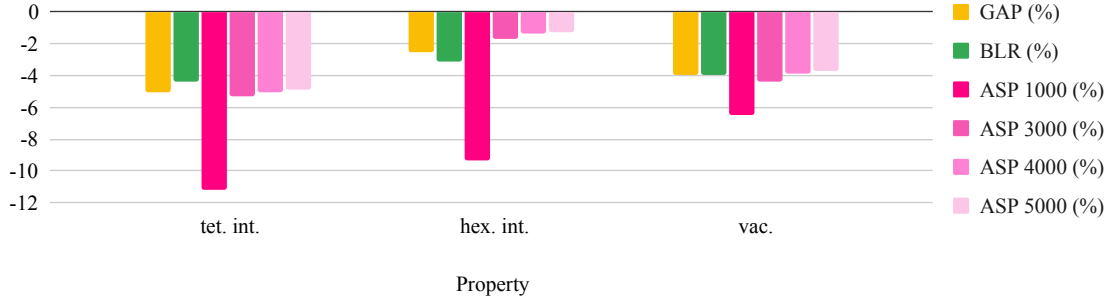


Fig. 5: Percentage error relative to the computed values in Table III for various silicon properties using GAP, BLR, and ASP (cf. III-B). The plot illustrates how the relative error of ASP decreases as the number of active basis functions increases, demonstrating a clear trend of improved accuracy.

Figure 6 presents the learning curve for ACE models trained on the water dataset, comparing the performance of OMP, ASP, and BLR solvers. Both OMP and ASP exhibit comparable mean absolute errors (MAE) while significantly outperforming BLR. In this case, OMP achieved slightly better accuracy than ASP while being more computationally efficient, hence we present all further results using only the OMP solver.

In the following numerical test, ASP and OMP models were initialized with a basis size of approximately 19,000, and training was terminated once the number of active basis functions reached 3,000, 9,000, and 12,000. Table IV compares the results obtained using ASP, OMP, and BLR with Cartesian Atomic Cluster Expansion (CACE) [19], which is a recently proposed framework that formulates atomic density expansions directly in Cartesian coordinates, bypassing the need for spherical harmonics. CACE $T = 0$ relies on local atomic features (similar to linear ACE), while $T = 1$ incorporates message passing to capture non-local interactions, improving accuracy at a higher computational cost.

Notably, the ACE models fitted using OMP require significantly fewer parameters than other models in Table IV. Specifically, the OMP solver achieves lower energy error than the CACE ($T = 0$) model while using less than 50% of the parameters. This is despite being a linear model, whereas CACE employs nonlinear tensor decompositions and a learnable radial basis. The larger force error suggests that tuning the regression weights may be beneficial, a process that should arguably also be automated in future work.

To illustrate the behavior of sparse solvers in this setting, Figure 7 shows the basis functions selected by the ASP solver for three-body interactions, with oxygen (O) as the central atom.

The selection pattern prioritizes O-H-H interactions over O-O-O and O-O-H, which intuitively should indeed have a the most important contribution to the total energy and forces. This selection pattern demonstrates that sparse, data-driven basis selection successfully identifies and prioritizes the most physically relevant interactions. Rather than following a hierarchical scheme, the solver autonomously captures the underlying physics of water, emphasizing the O-H-H bonds which are the building blocks of the water molecule [46]. Since we already have prior intuition about the interactions in water, the selected

pattern mainly serves to confirm it. However, it also illustrates the potential of sparse solvers to identify the most relevant interactions in systems where such intuition is lacking, helping to identify the most important interactions directly from the data.

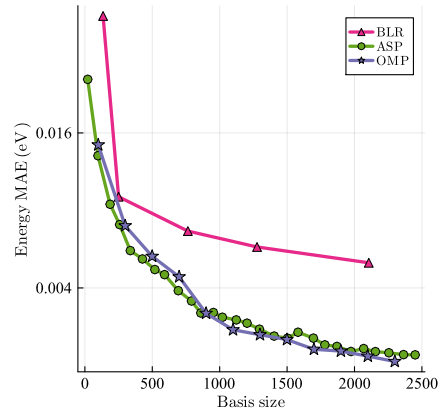


Fig. 6: Energy MAE vs. basis size for the Water dataset [18], comparing OMP, BLR, and ASP (cf. III-C). ASP and OMP significantly outperform BLR while using significantly fewer basis functions.

IV. CONCLUSION

We explored the use of sparse machine learning interatomic potentials (MLIPs) using active-set algorithms for automated data-driven feature selection. By integrating the `ActiveSetPursuit.jl` package into the Atomic Cluster Expansion (ACE) framework, we constructed sparse linear models that achieve both improved accuracy relative to dense ACE models as well as substantially reducing model complexity. The computational tests confirm that sparse optimization substantially reduces the need for manual hyperparameter tuning while improving model generalization.

V. ACKNOWLEDGEMENTS

The work was supported by the New Frontiers in Research Fund through an NFRF Exploration Grant, and by the Natural

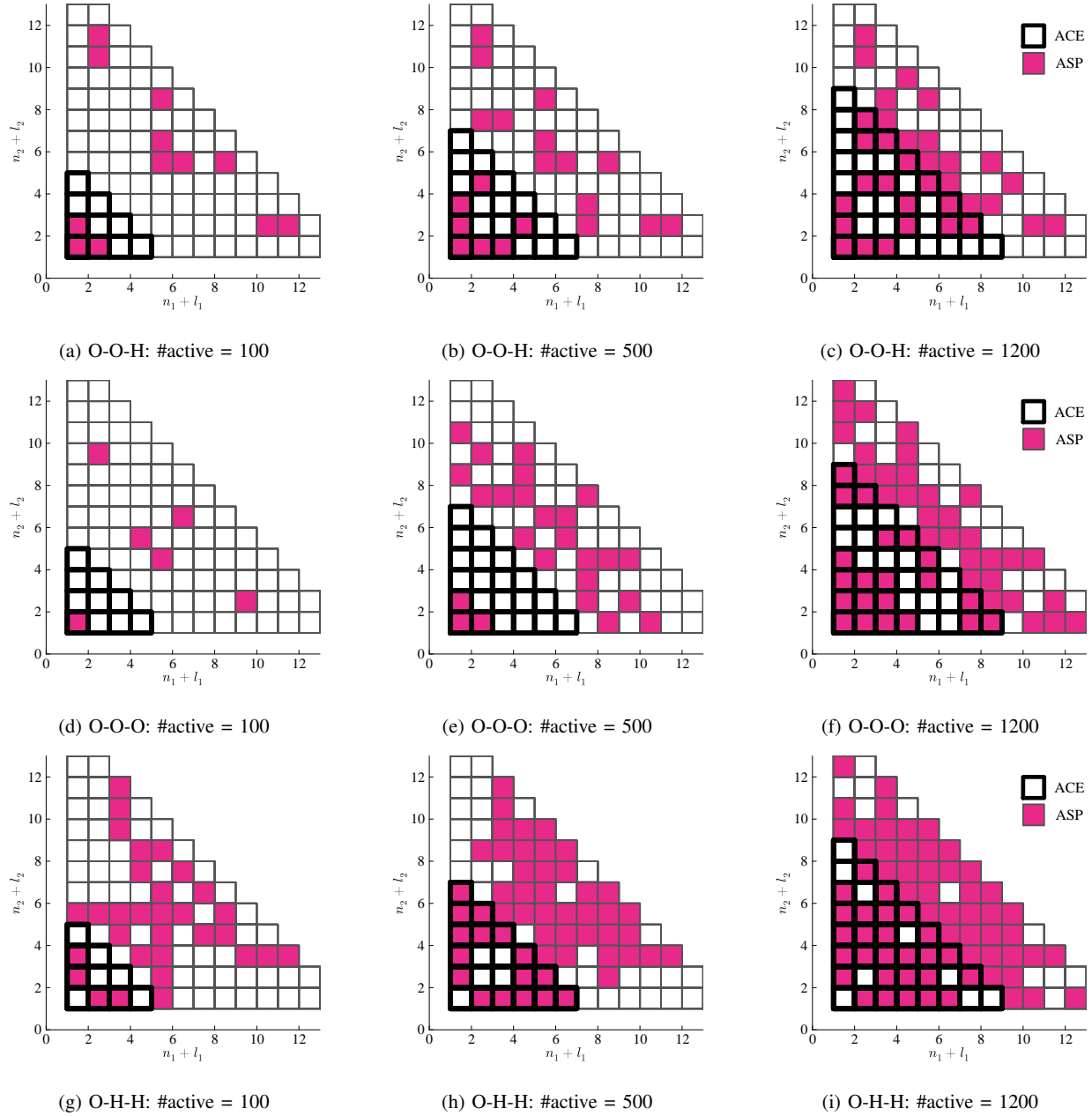


Fig. 7: Illustration of ASP and other (non-sparse) ACE solvers' gradual selection of three-body basis functions for the water dataset [18], with O as the center atom (cf. III-C). Each row corresponds to a different interaction type: O-H-H, O-O-O, and O-O-H. The results highlight the greater importance of resolving O-H interactions for accurately modeling the potential energy surface. This aligns with chemical intuition, as these bonds dominate water's structural and energetic properties due to their role in hydrogen bonding and intermolecular interactions.

Sciences and Engineering Research Council of Canada through an NSERC Discovery grant and an NSERC-NSF Collaboration on quantum science and artificial intelligence grant. CO is a partner in Symmetric Group LLP which licenses force fields commercially. The authors acknowledge helpful discussions with Gábor Csányi and Cas van der Oord.

APPENDIX

A. Radial Basis Functions

The general form of this one-particle basis is given by:

$$\phi_{\mathbf{n}\ell\mathbf{m}}(x_{ij}) = P_{\mathbf{n}\ell}(r_{ij}, Z_i, Z_j) Y_{\ell}^{\mathbf{m}}(\hat{\mathbf{r}}_{ij}),$$

TABLE IV: Test Mean Absolute Errors (MAE) for energy (E) per water molecule (in meV/H₂O) and force (in meV/Å) for models trained on a liquid water dataset from Ref. [18]. The cutoff radius r_{cut} of the atomic environment and the number of message passing layers T are listed. Despite being a linear model, the sparse solver achieves comparable accuracy with significantly fewer parameters, demonstrating the effectiveness of data-driven basis selection.

| Model | r_{cut} [Å] | Energy MAE (meV/atom) | Force MAE (meV/Å) | # Parameters |
|-----------------------|----------------------|-----------------------|-------------------|--------------|
| CACE [19] ($T = 1$) | 5.5 | 0.89 | 27 | 69320 |
| CACE [19] ($T = 0$) | 5.5 | 1.43 | 42 | 24572 |
| ACE (BLR) [52] | 5.5 | 1.86 | 76 | 19501 |
| ACE (OMP) | 5.5 | 2.02 | 88 | 3000 |
| ACE (OMP) | 5.5 | 1.43 | 63 | 9000 |
| ACE (OMP) | 5.5 | 1.35 | 59 | 12000 |

where Y_{ℓ}^m denote the complex or real spherical harmonics, while P_{nl} are radial basis functions with significant freedom of choice. The angular component \hat{r}_{ij} is embedded in the spherical harmonics, ensuring the parameterization is symmetric with respect to rotations. The radial basis function $R_{nl}(r_{ij}, Z_i, Z_j)$ is essential in modeling atomic interactions, and in the ACEpotentials.jl package, these bases are indexed only by \mathbf{n} , meaning $R_{nl} = R_{\mathbf{n}}$ for all l . This function is defined as

$$R_{\mathbf{n}}(r_{ij}, Z_i, Z_j) = f_{\text{env}}(r_{ij}, Z_i, Z_j) P_{\mathbf{n}}(y(r_{ij}, Z_i, Z_j)),$$

where y is an element-specific distance transformation designed to enhance spatial resolution, particularly near equilibrium bond lengths. A common form is

$$y(r_{ij}, Z_i, Z_j) = \left(1 + a \left(\frac{r}{r_0}\right)^q\right) \left(1 + \left(\frac{r}{r_0}\right)^{q-p}\right)^{-1},$$

with r_0 as an estimate of the equilibrium bond length and a chosen to maximize the gradient of y at $r = r_0$. Here, $P_{\mathbf{n}}$ is an orthogonal polynomial basis in the y -coordinates, typically chosen as Legendre polynomials to ensure even resolution over the y -domain. The function f_{env} serves as an envelope, specifying a cutoff radius r_{cut} . For the many-body basis, a typical choice is

$$f_{\text{env}}(r_{ij}, Z_i, Z_j) = y^2(y - y_{\text{cut}})^2,$$

where $y_{\text{cut}} = y(r_{\text{cut}}, Z_i, Z_j)$.

For the pair potential $V^{(1)}$, the default envelope is a modified Coulomb potential which ensures repulsive behavior as $r_{ij} \rightarrow 0$, while being continuously differentiable at the cutoff.

$$f_{\text{env}}(r_{ij}, Z_i, Z_j) = \left(\frac{r_{ij}}{r_0}\right)^{-1} - \left(\frac{r_{\text{cut}}}{r_0}\right)^{-1} + \left(\frac{r_{\text{cut}}}{r_0}\right)^{-2} \left(\frac{r_{ij}}{r_0} - \frac{r_{\text{cut}}}{r_0}\right).$$

For more information on the Atomic Cluster Expansion framework, the reader should refer to [52].

B. The BPDual Algorithm

The BPDual algorithm proposed by Friedlander and Saunders [27], is an active-set method specifically tailored for solving a class of quadratic programs (QP) that arise as the dual of Basis Pursuit Denoising (BPDN) problem. In this section

we will briefly review the main algorithm proposed. For more details the reader should refer to [27].

The optimal solutions of the basis pursuit denoising (BPDN) 3 and its dual QP are represented by \mathbf{x}^* and \mathbf{y}^* , respectively. The objective function of the dual QP and its gradient are given by:

$$\Phi(\mathbf{y}) = \frac{1}{2} \lambda \|\mathbf{y}\|_2^2 - \mathbf{b}^T \mathbf{y}, \quad \mathbf{g}(\mathbf{y}) = \lambda \mathbf{y} - \mathbf{b}$$

If $\lambda > 0$, $\Phi(\mathbf{y})$ is strictly convex, ensuring a unique solution \mathbf{y}^* . The vectors \mathbf{a}_j and \mathbf{e}_j represent the j -th columns of the matrix \mathbf{A} and the identity matrix, respectively. The j -th component of a vector \mathbf{z} is denoted by z_j . The support of a vector, denoted by \mathcal{S} , is the set of indices j where the corresponding element is non-zero: $x_j \neq 0$. The subvector $\mathbf{x}_{\mathcal{S}}$ contains only the non-zero components of the vector.

The BPDual algorithm is an active-set method. The active set method focuses on identifying constraints that are active (i.e., binding) at each iteration. For an estimated solution \mathbf{y} , a constraint is active if $\mathbf{a}_j^T \mathbf{y}$ lies at one of its bounds (i.e. $\mathbf{a}_j^T \mathbf{y} = 1$ or -1). The active set \mathcal{S} is a set of indices representing the active constraints at each iteration, which forms a submatrix of \mathbf{A} that has full column rank. For instance, for some permutation \mathbf{P}

$$\mathbf{A}\mathbf{P} = [\mathbf{S} \ \mathbf{N}] \quad \text{and} \quad \mathbf{S}^T \mathbf{y} = \pm \mathbf{1}.$$

The estimate \mathbf{y} is stationary if it satisfies the constraints $-1 \leq \mathbf{A}^T \mathbf{y} \leq 1$ and the objective gradient $\mathbf{g}(\mathbf{y})$ is a linear combination of active constraint gradients. Specifically, there exists $\mathbf{x}_{\mathcal{S}}$ such that:

$$\mathbf{S}\mathbf{x}_{\mathcal{S}} + \lambda \mathbf{y} = \mathbf{b} \quad \text{and} \quad \mathbf{S}^T \mathbf{y} = \pm \mathbf{1}. \quad (5)$$

These conditions imply that the current estimates (\mathbf{x}, \mathbf{y}) satisfy feasibility for the primal problem, with \mathbf{x} residing within the active constraints.

At each iteration, the algorithm seeks directions $\Delta \mathbf{x}_{\mathcal{S}}$ and $\Delta \mathbf{y}$ such that the updated $\mathbf{x}_{\mathcal{S}}$ and \mathbf{y} are stationary (i.e., they are feasible and satisfy the stationarity conditions 5). This is achieved by solving:

$$\min_{\Delta \mathbf{x}_{\mathcal{S}}} \|\mathbf{h} - \mathbf{S} \Delta \mathbf{x}_{\mathcal{S}}\|_2, \quad \Delta \mathbf{y} = \frac{\mathbf{h} - \mathbf{S} \Delta \mathbf{x}_{\mathcal{S}}}{\lambda},$$

where $\mathbf{h} = \mathbf{b} - \lambda \mathbf{y} - \mathbf{S} \mathbf{x}_{\mathcal{S}}$.

It's not worthy that for efficient computations, only the upper triangular part of a QR factorization of \mathbf{S} is updated at each iteration using the QRupdate.jl [28] package.

In the next step, a line search is performed to choose a step length $\alpha > 0$ to update \mathbf{x}_S and \mathbf{y} by taking steps $\mathbf{x}_S \rightarrow \mathbf{x}_S + \alpha \Delta \mathbf{x}_S$ and $\mathbf{y} \rightarrow \mathbf{y} + \alpha \Delta \mathbf{y}$, aiming to minimize $\phi(\mathbf{y})$. The step length $\alpha = 1$ is selected if possible, otherwise a constrained step is taken to avoid bound violations:

$$\alpha = \min \left\{ 1, \min_{j \notin S} \frac{\text{bound} - z_j}{\Delta z_j} \right\}.$$

If $\alpha < 1$, the line search encounters a constraint not currently in S . This constraint is added to S , ensuring that each new constraint introduced is linearly independent of the others in S . The linearly independence criterion is enforced as any newly encountered constraint must have a normal vector not lying in the span of S .

When $\alpha = 1$, the solution $\mathbf{y} + \Delta \mathbf{y}$ minimizes $\phi(\mathbf{y})$ on the current active set S . If improvement is possible by removing a constraint from S , the algorithm considers directions $\Delta \mathbf{y}$ that move \mathbf{y} away from an active constraint, maintaining feasibility. Consider an inequality constraint $q = S_p$ that is currently active at its lower bound, i.e., $a_q^T \mathbf{y} = -1$. To move away from this bound, we select a direction $\Delta \mathbf{y}$ satisfying $S^T \Delta \mathbf{y} = e_p$, ensuring $\Delta \mathbf{y}$ is a feasible direction that moves away from the active lower bound. Observe that:

$$g^T \Delta \mathbf{y} = (-S \mathbf{x}_S)^T \Delta \mathbf{y} = -\mathbf{x}_S^T S^T \Delta \mathbf{y} = -(\mathbf{x}_S)_p.$$

Thus, if $(\mathbf{x}_S)_p > 0$, moving in the direction $\Delta \mathbf{y}$ will improve the objective, allowing us to remove the constraint q from the active set.

Similarly, if the constraint q is active at its upper bound and $(\mathbf{x}_S)_p < 0$, we can improve the objective by moving in a direction $\Delta \mathbf{y}$ for which $S^T \Delta \mathbf{y} = -e_p$. In this case, we also remove constraint q from the active set. Hence, the Lagrange multipliers \mathbf{x}_S indicate which indices in the active set S should be removed to enable a reduction in the objective function. If none of the elements in \mathbf{x}_S have the appropriate sign, then the current point (\mathbf{x}, \mathbf{y}) is optimal.

C. Lasso Path

The homotopy approach, is a special case of parametric programming [8], aims to solve a sequence of LASSO problems, gradually adjusting a regularization parameter to trace a continuous path of solutions.

To apply the homotopy method to the dual problem 3 begins with a large initial value of $\lambda = \|\mathbf{A}^T \mathbf{b}\|$, where the solution \mathbf{x} is fully sparse. The parameter τ is then gradually decreased, following a continuous "path" of solutions that progressively allow more non-zero entries in \mathbf{x} . This path of solutions is often referred to as the *Lasso coefficient path*. At each iteration k , the algorithm solves a Lasso problem with the updated parameter λ_k via the BPDual algorithm.

As λ_k decreases, more coefficients in \mathbf{x} move from zero to non-zero values, revealing additional active variables in the model. Suppose \mathbf{y} is the optimal solution to the dual problem for a given τ , and let \mathbf{x}_S represent the vector of Lagrange multipliers for the active set S . The objective is to find the maximum reduction in λ such that S remains the optimal active set. Letting $\bar{\lambda} = \lambda - \alpha$, the corresponding optimal pair $(\bar{\mathbf{x}}_S, \bar{\mathbf{y}})$ satisfies the equations:

$$S \bar{\mathbf{x}}_S + \lambda \bar{\mathbf{y}} = \mathbf{b} \quad \text{and} \quad S^T \bar{\mathbf{y}} = \pm \mathbf{1}. \quad (6)$$

The homotopy algorithm calculates the largest allowable decrease in λ while maintaining feasibility of the current active set. To determine the direction in which the solution will change, we subtract the original optimality condition 5 from 6 and use the definition $\bar{\lambda} = \lambda - \alpha$, yielding:

$$S(\bar{\mathbf{x}}_S - \mathbf{x}_S) + \lambda(\bar{\mathbf{y}} - \mathbf{y}) - \alpha \mathbf{y} = 0, \quad S^T(\bar{\mathbf{y}} - \mathbf{y}) = 0.$$

By pre-multiplying the first equation by S^T and applying the second equation, we obtain:

$$S^T S(\bar{\mathbf{x}}_S - \mathbf{x}_S) = \alpha S^T \mathbf{y}.$$

This equation can be interpreted as the optimality condition for the following least-squares problem:

$$\bar{\mathbf{x}}_S = \mathbf{x}_S + \alpha \Delta \mathbf{x}, \quad \text{where } \Delta \mathbf{x} = \underset{\Delta \mathbf{x}}{\operatorname{argmin}} \|\mathbf{y} - S \Delta \mathbf{x}\|_2.$$

The direction of change for \mathbf{x}_S is thus independent of α . The maximum step α_j^x that can be taken without changing the sign of any component \mathbf{x}_j is given by:

$$\alpha_j^x = \begin{cases} -\mathbf{x}_j / \Delta \mathbf{x}_j & \text{if } j \in \mathcal{C}, \\ +\infty & \text{otherwise,} \end{cases}$$

where $\mathcal{C} = \{j \mid \operatorname{sign}(\mathbf{x}_j) = -\operatorname{sign}(\Delta \mathbf{x}_j)\}$. Thus, the feasible step size α cannot be larger than $\alpha^x = \min_j \alpha_j^x$.

As λ decreases to $\bar{\lambda}$, it is also necessary to assess the impact on \mathbf{y} , particularly with respect to the constraints $-1 \leq A^T \mathbf{y} \leq 1$. Subtracting $\bar{\mathbf{y}}$ from both sides and using the definition of $\Delta \mathbf{x}$, we obtain:

$$(\lambda - \alpha)(\bar{\mathbf{y}} - \mathbf{y}) = \mathbf{b} - \lambda \mathbf{y} - S \mathbf{x}_S + \alpha(\mathbf{y} - S \Delta \mathbf{x}).$$

Due to the optimality of the current pair (\mathbf{x}, \mathbf{y}) , we have:

$$\bar{\mathbf{y}} = \mathbf{y} + \frac{\alpha}{\lambda - \alpha} \Delta \mathbf{y}, \quad \text{where } \Delta \mathbf{y} := \mathbf{y} - S \Delta \mathbf{x}.$$

This expression represents the residual in the least-squares problem. Consequently, the change in constraints can be captured by:

$$\bar{\mathbf{z}} = \mathbf{z} + \frac{\alpha}{\lambda - \alpha} \Delta \mathbf{z}, \quad \text{where } \mathbf{z} := A^T \mathbf{y} \quad \text{and} \quad \Delta \mathbf{z} := A^T \Delta \mathbf{y}.$$

The maximum feasible step α_j^z without violating a constraint $j \notin S$ is:

$$\alpha_j^z = \begin{cases} \frac{\lambda(1 - \mathbf{z}_j)}{\Delta \mathbf{z}_j - \mathbf{z}_j + 1} & \text{if } \Delta \mathbf{z}_j > 0, \\ \frac{\lambda(-1 - \mathbf{z}_j)}{\Delta \mathbf{z}_j - \mathbf{z}_j - 1} & \text{if } \Delta \mathbf{z}_j < 0, \\ +\infty & \text{otherwise,} \end{cases}$$

Thus, the feasible step size α cannot exceed $\alpha^z = \min_{j \notin S} \alpha_j^z$. The total allowable reduction in λ is therefore $\alpha = \min\{\alpha^x, \alpha^z\}$.

In each iteration, the homotopy algorithm updates the active set and adjusts the solution (\mathbf{x}, \mathbf{y}) by taking the largest feasible step α , driving the optimization towards minimizing the objective function while adhering to feasibility constraints.

D. Orthogonal Matching Pursuit

Orthogonal Matching Pursuit (OMP) is a greedy algorithm for finding a sparse solution to the linear system $Ax = b$. OMP constructs the support of x iteratively, adding one nonzero component at each step. Initially, the solution vector is set to $x_0 = 0$, the active set is $\mathcal{S}_0 = \emptyset$, and the residual is $r_0 = b$. At each iteration k , OMP identifies the column a_i of A that is most correlated with the current residual r_{k-1} . Specifically, it selects the index i that maximizes the absolute value of the following inner product, $i = \arg \max_i |\langle a_i, r_{k-1} \rangle|$. The active set is then updated as $\mathcal{S}_k = \mathcal{S}_{k-1} \cup \{i_k\}$. The algorithm computes the new solution x_k by minimizing the residual norm $\|b - Ax\|_2$ over vectors supported on \mathcal{S}_k . Finally, the residual is updated as $r_k = b - Ax_k$. The algorithm enforces the orthogonality of r_k with respect to the columns of A in the current support, ensuring that once a column is selected, it will not be chosen again. This process repeats until a stopping criterion, such as a sufficiently small residual norm, is met.

E. BRR Posterior Derivation

Starting with the Gaussian likelihood and prior, the posterior distribution for the coefficients x is derived using Bayes' theorem:

$$p(x | b, A, \alpha, \lambda) \propto p(b | A, x, \lambda) p(x | \alpha).$$

Detailed algebra shows that the posterior is Gaussian with covariance

$$\Sigma = (\alpha I + \lambda A^\top A)^{-1},$$

and mean

$$\hat{x} = \lambda \Sigma A^\top b.$$

The marginal likelihood (evidence) is given by:

$$p(b | A, \alpha, \lambda) = \int p(b | x, A, \lambda) p(x | \alpha) dx.$$

Taking the logarithm yields:

$$\begin{aligned} \ln p(b | A, \alpha, \lambda) = & -\frac{m}{2} \ln(2\pi) + \frac{1}{2} \ln |\Sigma| \\ & -\frac{\lambda}{2} \|b - A\hat{x}\|^2 - \frac{\alpha}{2} \|\hat{x}\|^2. \end{aligned}$$

This marginal log-likelihood is maximized with respect to α (or α in the ARD case) and λ , typically using optimization methods such as BFGS or L-BFGS.

F. Truncated Singular Value Decomposition (TSVD) Post-Processing

The ASP solver applies ℓ_1 -regularization, which promotes sparsity but can also shrink the recovered coefficients excessively toward zero. To mitigate this effect and improve numerical stability, we apply a post-processing step using truncated singular value decomposition (TSVD).

Given the selected subset of basis functions S , let A_S denote the reduced design matrix corresponding to these basis functions, and let x be the final iterate obtained from ASP. The TSVD-based refinement is performed as follows:

- 1) Compute the singular value decomposition (SVD) of the matrix A_S :

$$A_S = U \Sigma V^T,$$

where $U \in \mathbb{R}^{m \times r}$ and $V \in \mathbb{R}^{n \times r}$ are orthonormal matrices, and $\Sigma \in \mathbb{R}^{r \times r}$ is a diagonal matrix containing the singular values $\sigma_1 \geq \sigma_2 \geq \dots \geq \sigma_r$.

- 2) Define a truncation threshold σ_{\min} , typically chosen as a fraction of the largest singular value (e.g., $\sigma_{\min} = \epsilon \sigma_1$ for some small ϵ). Retain only the singular values satisfying $\sigma_i > \sigma_{\min}$, and form the truncated SVD:

$$A_S^{(\text{TSVD})} = U_k \Sigma_k V_k^T,$$

where k is the number of singular values exceeding σ_{\min} , and U_k, Σ_k, V_k are the corresponding truncated matrices.

- 3) Project the solution x onto the lower-rank subspace:

$$x_{\text{TSVD}} = V_k \Sigma_k^{-1} U_k^T b.$$

By applying TSVD, we filter out small singular values that introduce numerical instability while preserving the dominant components of x . This step counteracts the over-shrinkage induced by the ℓ_1 -regularization and ensures a more stable and accurate recovery of the coefficient vector.

REFERENCES

- [1] M. Bachmayr, G. Csanyi, G. Dusson, R. Drautz, S. Etter, C. Oord, and C. Ortner. Atomic cluster expansion: Completeness, efficiency and stability. *J. Comput. Phys.*, 454, 2022.
- [2] M. Bachmayr, G. Dusson, C. Ortner, and J. Thomas. Polynomial approximation of symmetric functions. *Math. Comp.*, 93:811–839, 2024.
- [3] A. P. Bartók, M. C. Payne, R. Kondor, and G. Csányi. Gaussian approximation potentials: The accuracy of quantum mechanics, without the electrons. *Phys. Rev. Lett.*, 104:136403, Apr 2010.
- [4] Albert P. Bartók, James Kermode, Noam Bernstein, and Gábor Csányi. Machine learning a general-purpose interatomic potential for silicon. *Phys. Rev. X*, 8:041048, Dec 2018.
- [5] Albert P. Bartók, Risi Kondor, and Gábor Csányi. On representing chemical environments. *Physical Review B*, 87(18), May 2013.
- [6] Jörg Behler. Atom-centered symmetry functions for constructing high-dimensional neural network potentials. *The Journal of Chemical Physics*, 134(7):074106, 02 2011.
- [7] N. Bernstein, G. Csányi, and V. Deringer. De novo exploration and self-guided learning of potential-energy surfaces. *npj Computational Materials*, 5, 12 2019.
- [8] Dimitris Bertsimas and John Tsitsiklis. *Introduction to Linear Optimization*. 01 1998.
- [9] Bastiaan J. Braams and Joel M. Bowman and. Permutationally invariant potential energy surfaces in high dimensionality. *International Reviews in Physical Chemistry*, 28(4):577–606, 2009.
- [10] K. Burke. Perspective on density functional theory. *The Journal of chemical physics*, 136:150901, 04 2012.
- [11] Emmanuel Candes and Michael Wakin. Wakin, m.b.: An introduction to compressive sampling. *IEEE Signal Process. Mag.*, 25(2), 21-30. *Signal Processing Magazine, IEEE*, 25:21 – 30, 04 2008.

- [12] Emmanuel J. Candès, Justin K. Romberg, and Terence Tao. Stable signal recovery from incomplete and inaccurate measurements. *Communications on Pure and Applied Mathematics*, 59(8):1207–1223, 2006.
- [13] Tony F. Chan. Rank revealing qr factorizations. *Linear Algebra and its Applications*, 88-89:67–82, 1987.
- [14] Chi Chen, Weike Ye, Yunxing Zuo, Chen Zheng, and Shyue Ong. Graph networks as a universal machine learning framework for molecules and crystals. *Chemistry of Materials*, 31, 04 2019.
- [15] Chi Chen, Yunxing Zuo, Weike Ye, Xiang-Guo Li, and Shyue Ong. Learning properties of ordered and disordered materials from multi-fidelity data. *Nature Computational Science*, 1:46–53, 01 2021.
- [16] Scott Shaobing Chen, David L. Donoho, and Michael A. Saunders. Atomic decomposition by basis pursuit. *SIAM Journal on Scientific Computing*, 20(1):33–61, 1998.
- [17] Scott Shaobing Chen, David L. Donoho, and Michael A. Saunders. Atomic decomposition by basis pursuit. *SIAM Review*, 43(1):129–159, 2001.
- [18] B. Cheng, E. A. Engel, J. Behler, C. Dellago, and M. Ceriotti. Ab initio thermodynamics of liquid and solid water. *Proceedings of the National Academy of Sciences*, 116(4):1110–1115, 2019.
- [19] Bingqing Cheng. Cartesian atomic cluster expansion for machine learning interatomic potentials. *npj Computational Materials*, 10, 07 2024.
- [20] Stewart J. Clark, Matthew D. Segall, Chris J. Pickard, Phil J. Hasnip, Matt I. J. Probert, Keith Refson, and Mike C. Payne. First principles methods using castep. *Zeitschrift für Kristallographie - Crystalline Materials*, 220(5-6):567–570, 2005.
- [21] M. S. Daw, S. M. Foiles, and M. I. Baskes. The embedded-atom method: a review of theory and applications. *Materials Science Reports*, 9(7):251–310, 1993.
- [22] Marc Peter Deisenroth, A. Aldo Faisal, and Cheng Soon Ong. *Mathematics for Machine Learning*. Cambridge University Press, 2020.
- [23] Volker L. Deringer, Noam Bernstein, Albert P. Bartók, Matthew J. Cliffe, Rachel N. Kerber, Lauren E. Marbella, Clare P. Grey, Stephen R. Elliott, and Gábor Csányi. Realistic atomistic structure of amorphous silicon from machine-learning-driven molecular dynamics. *The Journal of Physical Chemistry Letters*, 9(11):2879–2885, Jun 2018.
- [24] Volker L. Deringer, Miguel A. Caro, and Gábor Csányi. Machine learning interatomic potentials as emerging tools for materials science. *Advanced Materials*, 31(46):1902765, 2019.
- [25] Ralf Drautz. Atomic cluster expansion for accurate and transferable interatomic potentials. *Phys. Rev. B*, 99:014104, Jan 2019.
- [26] Laurent El Ghaoui and Hervé Lebret. Robust solutions to least-squares problems with uncertain data. *SIAM Journal on Matrix Analysis and Applications*, 18(4):1035–1064, 1997.
- [27] M. P. Friedlander and M. A. Saunders. A dual active-set quadratic programming method for finding sparse least-squares solutions. Technical report, Department of Computer Science, University of British Columbia, July 30 2012.
- [28] Michael P. Friedlander and contributors. Qrupdate.jl - a julia package for updating qr factorizations. <https://github.com/mpf/QRupdate.jl>, 2012. Accessed: 2024-10-29.
- [29] Michael P. Friedlander and Michael A. Saunders. Active-set pursuit: an active-set solver for basis pursuit and related sparse optimization problems. <https://github.com/MPF-Optimization-Laboratory/asp>.
- [30] William Karush. Minima of functions of several variables with inequalities as side conditions. Master’s thesis, Department of Mathematics, University of Chicago, Chicago, IL, USA, 1939.
- [31] H. W. Kuhn and A. W. Tucker. *Nonlinear Programming*, pages 481–492. University of California Press, Berkeley, 1951.
- [32] Shao-Bo Lin, Xin Guo, and Ding-Xuan Zhou. Distributed learning with regularized least squares. *Journal of Machine Learning Research*, 18(92):1–31, 2017.
- [33] David J. C. MacKay. *Bayesian Non-Linear Modeling for the Prediction Competition*, pages 221–234. Springer Netherlands, Dordrecht, 1996.
- [34] David John Cameron MacKay. Bayesian interpolation. *Neural Computation*, 4:415–447, 1992.
- [35] Stéphane Mallat. *A Wavelet Tour of Signal Processing, Third Edition: The Sparse Way*. Academic Press, Inc., USA, 3rd edition, 2008.
- [36] B. K. Natarajan. Sparse approximate solutions to linear systems. *SIAM Journal on Computing*, 24(2):227–234, 1995.
- [37] MR Osborne, B Presnell, and BA Turlach. A new approach to variable selection in least squares problems. *IMA Journal of Numerical Analysis*, 20(3):389–403, 07 2000.
- [38] Y.C. Pati, R. Rezaiifar, and P.S. Krishnaprasad. Orthogonal matching pursuit: recursive function approximation with applications to wavelet decomposition. In *Proceedings of 27th Asilomar Conference on Signals, Systems and Computers*, pages 40–44 vol.1, 1993.
- [39] F. Pedregosa, G. Varoquaux, A. Gramfort, V. Michel, B. Thirion, O. Grisel, M. Blondel, P. Prettenhofer, R. Weiss, V. Dubourg, J. Vanderplas, A. Passos, D. Cournapeau, M. Brucher, M. Perrot, and E. Duchesnay. Scikit-learn: Machine learning in Python. *Journal of Machine Learning Research*, 12:2825–2830, 2011.
- [40] Patrick Reiser, Marlen Neubert, André Eberhard, Luca Torresi, Chen Zhou, Chen Shao, Houssam Metni, Clint Hoesel, Henrik Schopmans, Timo Sommer, and Pascal Friederich. Graph neural networks for materials science and chemistry. *Communications Materials*, 3, 11 2022.
- [41] Alexander Shapeev. Moment tensor potentials: A class of systematically improvable interatomic potentials. *Multi-scale Modeling & Simulation*, 14, 12 2015.
- [42] J. Tersoff. New empirical approach for the structure and energy of covalent systems. *Phys. Rev. B*, 37:6991–7000, Apr 1988.
- [43] A.P. Thompson, L.P. Swiler, C.R. Trott, S.M. Foiles, and G.J. Tucker. Spectral neighbor analysis method for automated generation of quantum-accurate interatomic

- potentials. *Journal of Computational Physics*, 285:316–330, 2015.
- [44] Robert Tibshirani. Regression shrinkage and selection via the lasso. *Journal of the royal statistical society series b-methodological*, 58:267–288, 1996.
 - [45] Robert Tibshirani. Regression shrinkage and selection via the lasso. *Journal of the Royal Statistical Society. Series B (Methodological)*, 58(1):267–288, 1996.
 - [46] John Tatini Titantah and Mikko Karttunen. Water dynamics: Relation between hydrogen bond bifurcations, molecular jumps, local density & hydrophobicity. *Scientific Reports*, 3(1):2991, Oct 2013.
 - [47] Tina Torabi. Activesetpursuit.jl: A julia implementation of active set pursuit algorithms for sparse optimization. <https://github.com/MPF-Optimization-Laboratory/ActiveSetPursuit.jl>, 2024. Accessed: 2024-11-05.
 - [48] Sara van de Geer, Peter Bühlmann, Ya’acov Ritov, and Ruben Dezeure. On asymptotically optimal confidence regions and tests for high-dimensional models. *The Annals of Statistics*, 42(3):1166 – 1202, 2014.
 - [49] Ewout van den Berg and Michael P. Friedlander. Probing the pareto frontier for basis pursuit solutions. *SIAM Journal on Scientific Computing*, 31(2):890–912, 2009.
 - [50] Cas van der Oord, Matthias Sachs, D’avid P’eter Kov’acs, Christoph Ortner, and Gábor Csányi. Hyperactive learning for data-driven interatomic potentials. *Npj Computational Materials*, 9, 2022.
 - [51] Robert Vanderbei. Linear programming: Foundations and extensions. *Journal of the Operational Research Society*, 49, 03 2002.
 - [52] W. C. Witt, C. van der Oord, E. Gelžinytė, T. Järvinen, A. Ross, J. P. Darby, C. Hin Ho, W. J. Baldwin, M. Sachs, J. Kermode, N. Bernstein, G. Csányi, and C. Ortner. ACEpotentials.jl: A Julia implementation of the atomic cluster expansion. *The Journal of Chemical Physics*, 159(16):164101, 10 2023.
 - [53] Tian Xie and Jeffrey C. Grossman. Crystal graph convolutional neural networks for an accurate and interpretable prediction of material properties. *Phys. Rev. Lett.*, 120:145301, Apr 2018.
 - [54] Cun-Hui Zhang and Stephanie S. Zhang. Confidence intervals for low dimensional parameters in high dimensional linear models. *Journal of the Royal Statistical Society Series B: Statistical Methodology*, 76(1):217–242, 07 2013.
 - [55] Y. Zuo, C. Chen, X. Li, Z. Deng, Y. Chen, J. Behler, G. Csányi, A. Shapeev, A. Thompson, M. A. Wood, and Shyue P. Ong. Performance and cost assessment of machine learning interatomic potentials. *The Journal of Physical Chemistry A*, 124(4):731–745, Jan 2020.